Dissipative particle dynamics simulations of tri-block co-polymer and water: Phase diagram validation and microstructure identification

Dissipative Particle Dynamics simulations of tri-block co-polymer and water: phase diagram validation and microstructure identification

Hermes Droghetti[1], Ignacio Pagonabarraga[2,3], Paola Carbone[4], Pietro Asinari[5] and Daniele Marchisio[1]

[1] Department of Applied Science and Technology, Institute of Chemical Engineering, Politecnico di Torino, C.so Duca degli Abruzzi 24, 10129 Torino, Italy

[2] Departament de Física de la Matèria Condensada, Universitat de Barcelona, Barcelona, Spain

[3] CECAM Centre Européen de Calcul Atomique et Moléculaire, École Polytechnique Fédérale de Lausanne (EPFL), Lausanne, Switzerland

[4] School of Chemical Engineering and Analytical Science, The University of Manchester, Oxford Road, Manchester M13 9PL, United Kingdom

[5] Department of Energy, Politecnico di Torino, C.so Duca degli Abruzzi 24, 10129 Torino, Italy

Abstract:

In this study the phase diagram of Pluronic L64 and water is simulated via DPD. The peculiar structures that form when the concentration varies from dilute to dense (i.e. spherical and rod-like micelles, hexagonal and lamellar phases, as well as reverse micelles) are recognized and predictions are found to be in in good agreement with experiments. A novel clustering algorithm is used to identify the structures formed, characterize them in terms of radius of gyration and aggregation number and cluster mass distributions. Non-equilibrium simulations are also performed, in order to predict how structures are affected by shear, both via qualitative and quantitative analyses. Despite the well-known scaling problem that results in unrealistic shear rates in real units, results show that non-Newtonian behaviors can be predicted by DPD and associated to variations of the observed microstructures.

1. Introduction

Structured fluids are colloidal dispersions typically obtained by mixing an organic phase with an aqueous one with the help of surfactant molecules. Within the fluid, micro- or nano-phases characterized by well-defined microstructures can be obtained, varying the nature and the concentration of the components, as well as the mixing rate. The simplest example of structured fluids, that can produce a rich variety of microstructures, is the mixture formed by amphiphilic surfactants and water. As well-known, surfactant molecules self-assemble together in water, with the hydrophilic part creating a shell around the hydrophobic core and forming different microstructures, ranging from spherical and cylindrical micelles, to hexagonal and lamellar structures. Phase diagrams are built to forecast when a specific microstructure is formed and their derivation (from scattering and rheological experiments) is a quite standard procedure in this research area. However, when a structured fluid is deformed, the fate of the involved microstructures is less explored, and this work aims at addressing this issue by using a computational model.

The self-assembly of large surfactant molecules, as well as the effect of shear on the observed microstructures, take place on timescales which are commonly not accessible by traditional All-Atom Molecular Dynamics (AAMD). Therefore, mesoscopic models, such as Dissipative Particle Dynamics (DPD), can be used to investigate wider timescale ranges and highlight peculiar behaviors of such fluids, even though the molecular resolution of the model is reduced[1]. DPD describes the interaction between beads, representative of clusters of atoms and molecules, using a bead-spring model, repulsive soft potentials combined with stochastic and dissipative forces. Prhashanna et al., Cheng et al., Zhen et al., Cao et al., Li et al. already discussed and validated the reliability of DPD to predict the formation of micelles, at thermodynamic equilibrium, and microstructures in systems composed by water and surfactants[2-6]. Also, complete phase diagrams can be obtained for ternary compounds as described by Wang et al., Son et al., and Yuan et al.[7-9]. When a mechanical perturbation is applied (like in a mixing tank), shear stresses induce deformation of the microstructure that can

lead to phase transitions[10-12]. One of the most popular structured fluids investigated in the literature, both via experiments and simulations[18-36], is composed of water and the triblock co-polymer of polyethylene oxide (PEO)-polypropylene oxide (PPO)-polyethilene oxide (PEO), under the commercial name Pluronic®, by BASF. This nonionic co-polymer can be manufactured varying the number of EO and PO monomers, such that the length of the hydrophilic (PEO) and hydrophobic (PPO) blocks can be varied to tune its amphiphilic properties, hence its phase diagram together with the temperature. Spherical and cylindrical micelles are present at low concentration, soft-gels are formed at slightly higher concentrations and oriented lamellar structures are observed at very high concentrations [37, 38]. Due to their incredibly wide range of applications and their relative simple structure, different Pluronic, named with different labels based on the length of the repeating units, such as P84, L64, F127, P123 have been investigated from the computational point of view using DPD under both equilibrium and non-equilibrium simulations[2, 39 - 41].

Shear effects on microstructures can be proved by the change in the apparent viscosity shown by water-surfactant systems at different shear rates as described by Newby et al., and Youssy et al., where the rheological properties of Poloxamer 407 in aqueous solutions were investigated[13, 14]. Phase transitions, changes in orientation, deformation and coalescence of micelles are examples of the phenomena involved when these fluids are subjected to shear[15]. The transition from spherical to cylindrical or worm/rod-like micelles is also a very common event. These elongated structures can create a structured network or align themselves according to the direction of the flow, such that the overall behavior of the fluid is non-Newtonian. At high concentration, the effect of the shear on complex systems plays an even more relevant role. For example, Gentile et al. demonstrated that lamellar phases could rearrange their shape producing multilamellar vesicles, with a resulting non-Newtonian behavior[16, 17].

This work aims at predicting a full phase diagram for the system described, highlighting different morphologies and quantitatively assess their shape and number, via a clustering algorithm. Also, we investigated the effect that an applied shear has on the equilibrium microstructures and its relationship

with the changes in the resulting rheological behavior. This was done here by simulating a specific Pluronic co-polymer known as L64, i.e. $((EO)_{13}(PO)_{30}(EO)_{13})$, using DPD, for which a set of parameters, optimized against the experimental equilibrium phase diagram, are available[42]. The shear flow is simulated by means of non-equilibrium DPD simulations and its effect on the observed morphologies is quantified via a cluster analysis that allows to count and identify the geometry of the polymer structures. Finally, the apparent viscosity of the structured fluid is calculated and its variation with the liquid microstructures is explained.

2. Model description

The mesoscopic technique named Dissipative Particle Dynamics (DPD) was firstly introduced by Hoogerbrugge and Koelman as an alternative to lattice-gas automata schemes[43]. The original model was corrected and improved by Groot, Warren, Español and Pagonabarraga [44-46]. Among its wide range of possible applications, DPD can be used to simulate shear effects on complex fluids due to the peculiarity of preserving hydrodynamic interactions[2, 47,48]. In a DPD simulation, interacting beads are representative of clusters of atoms or molecules. The interaction between beads can be described with Langevin dynamics:

$$\frac{d\boldsymbol{r_i}}{dt} = \boldsymbol{v_i}, \tag{1}$$

$$\frac{d\boldsymbol{v_i}}{dt} = \boldsymbol{f_i}, \tag{2}$$

where $\boldsymbol{f_i}$ is given by:

$$\boldsymbol{f_i} = \sum_{\boldsymbol{j \neq i}} (\boldsymbol{F_{ij}^C} + \boldsymbol{F_{ij}^R} + \boldsymbol{F_{ij}^D}), \tag{3}$$

the force acting on each DPD particle i, $\boldsymbol{f_i}$, is the sum of a conservative, dissipative and stochastic term. The conservative force can be described as follows:

$$\boldsymbol{F_{ij}^C} = \begin{cases} a_{ij}\left(1 - \frac{r_{ij}}{r_c}\right)\hat{\boldsymbol{r}}_{ij}, & r_{ij} < r_c \\ 0, & r_{ij} \geq r_c \end{cases}, \tag{4}$$

where a_{ij} represents the conservative soft potential parameter, $\boldsymbol{r_{ij}} = \boldsymbol{r_i} - \boldsymbol{r_j}$ is the relative distance between two beads *i* and *j*, $r_{ij} = |\boldsymbol{r_{ij}}|$, and $\hat{\boldsymbol{r}}_{\boldsymbol{ij}} = \frac{\boldsymbol{r_{ij}}}{|r_{ij}|}$ and r_c is the cut-off radius, a characteristic length. The dissipative force is described as follows:

$$\boldsymbol{F_{ij}^D} = -\gamma w^D(r_{ij})(\hat{\boldsymbol{r}}_{\boldsymbol{ij}} \cdot \boldsymbol{v_{ij}})\,\hat{\boldsymbol{r}}_{\boldsymbol{ij}}\,, \tag{5}$$

where γ represents the dissipative coefficient acting as an artificial drag on the beads, w^D is a weight function that defines the maximum range of application of the force, and $\boldsymbol{v_{ij}}$ is the relative velocity between two beads *i* and *j*. Its dependence on the velocity of the beads allows DPD to act as a thermostat in regulating the temperature of the system[1]. The stochastic force can be described as follows:

$$\boldsymbol{F_{ij}^R} = \sigma w^R(r_{ij})\,\zeta_{ij}\Delta t^{-1/2}\hat{\boldsymbol{r}}_{\boldsymbol{ij}}, \tag{6}$$

where σ is the stochastic coefficient, w^R is again a weight function, ζ_{ij} is a random fluctuating variable with zero mean and unitary variance and Δt is the simulation timestep. The weight functions and the stochastic and dissipative coefficients are connected by the fluctuation-dissipation theorem[1] as follows:

$$w^D(r_{ij}) = \left[w^R(r_{ij})\right]^2 = \begin{cases} \left(1 - \frac{r_{ij}}{r_c}\right)^2, & r_{ij} < r_c \\ 0, & r_{ij} \geq r_c \end{cases}, \tag{7}$$

$$\sigma^2 = 2\gamma k_B T, \tag{8}$$

where k_B is the Boltzmann constant and T is the temperature of the system. This last equation clarifies that the choice of one of the interaction parameter implies that the other is already defined. Bonded interactions are needed to maintain the topology of the polymer chain. Two types of bonded potentials have been investigated in this study: harmonic and finite-extensible nonlinear-elastic (FENE) potentials. The harmonic potential is described as follows:

$$E_{Harm} = K_{Harm}\,(r_{ij} - r_e)^2, \qquad (9)$$

where K_{Harm} is the harmonic constant and r_e is the equilibrium distance between two connected beads, while the FENE potential is:

$$E_{FENE} = -K_{FENE}\,r_e{}^2 \ln\left[1 - \left(\frac{r_{ij}}{r_e}\right)^2\right], \qquad (10)$$

where K_{FENE} is the FENE bond constant, r_e is the equilibrium distance and r is the distance between two beads.

The viscosity of a DPD system has been calculated using the non-equilibrium method known as Lees-Edwards boundary conditions (LEBC)[49], where different values of shear stress can be obtained through the application of different velocities on the beads that are close to the boundaries (top and bottom) of the simulation box. The maximum value of the velocity at the top of the box is equal to $\dot{\gamma} l$, where $\dot{\gamma}$ is the shear value imposed on the system and l is the length of the box. If the conservation of momentum is respected, a linear velocity profile, across the simulation box, is obtained. The magnitude of the shear stress should lead to velocities that are larger than the thermal velocity of the beads, leading to meaningfully observable shear flows in computational studies. Also, periodic boundary conditions were used to ensure that the total number of beads and their behavior were consistent with the streaming effect. The viscosity can then be obtained via the following relationship:

$$\mu_{DPD} = -\frac{P_{xy}}{\dot{\gamma}}, \tag{11}$$

where $\dot{\gamma}$ is the imposed shear rate, while P_{xy} is the non-zero, *xy* non-diagonal component of the stress tensor. LEBC allows to obtain rheograms, linking any changes in the fluid morphology, due to the application of the shear, to changes in its viscosity. It must be however highlighted that, fixed one value of the dissipative coefficient, γ, one drawback of the method is that only a limited range of shear is applicable, without having anomalies in the viscosity, as it is possible to observe in the Supporting Information.

A final remark regards the conversion between DPD and real units. In order to compare the results of DPD simulations with experiments, it is necessary to define a conversion benchmark, such as a set of values representing physical quantities. Having in mind that DPD beads are representative of different clusters of atoms/molecules with the same size and weight, three variables can be used to define one possible conversion set (i.e. a length, a mass and a kinetic energy). The length, defined as a cut-off radius, represents the maximum level of interaction between DPD beads, the mass represents the number of particles clustered into one bead and the kinetic energy is an indicator of the thermal velocity of the beads. DPD simulations are performed using these parameters normalized to unity. If this set is fixed, all the remaining parameters can be obtained by their combination. Although this conversion set of parameters is producing consistent results in evaluating equilibrium properties, the same does not apply in non-equilibrium conditions. The conversion of DPD values into real physical units, according to the equilibrium conversion set, could produce unrealistic values for non-equilibrium quantities, such as form example the actual shear rate applied (similarly to what happens in non-equilibrium AAMD). It is also necessary to say that, given this set of parameters and types of interaction, chain-crossing is allowed. This could also bring to deviations from real, physical quantities. Despite all these limitations we think the present analysis is useful and can generate interesting results.

3. Simulation Details

The simulated systems, composed by DPD beads, represent water molecules and Pluronic L64 chains. Two sets of simulations have been performed, in order to assess both equilibrium and non-equilibrium properties. The computational code used for this purpose was LAMMPS[50] and graphical outputs were produced using VMD[51].

The DPD parameters used to simulate the polymer chains were obtained from the literature[2]. The level of coarse-graining adopted to describe the Pluronic L64 chains is 4.3 for the EO repeated units and 3.3 for the PO repeated units. This means that one coarse-grained bead of EO contains 4.3 atomistic EO monomers and the same conversion procedure applies for PO. Using this set of parameters, Pluronic L64 chains are composed by 15 beads and simulated as $A_3B_9A_3$ DPD chains, where A is the coarse-grained bead for the EO unit and B is the coarse-grained bead for the PO one. Simulations of different concentrations of Pluronic L64 in water were performed by varying the number of beads of the two components, keeping the total number of beads in each box fixed (e.g. for a system composed by 81000 beads, if 50% is composed by water, 40500 spherical beads are water-type). Bonded and non-bonded interactions between beads are accounted for in the DPD model. The former were described using both harmonic and FENE potentials, while the latter are reported in Table 1. All values are reported in DPD units.

The dissipative parameter γ was set equal to 4.5 (in DPD units) for all the species, while the stochastic parameter σ was set equal to 3, according to the fluctuation-dissipation theorem [1] when the value of k_BT is equal to 1. Simulation boxes of different sizes were tested, from 20×20×20 cut-off radii to 40×40×40 cut-off radii. The simulation box of 30×30×30 cut-off radii was found to be a reasonable compromise between reduction of simulation box artifacts and acceptable simulation times. The initial configuration of the system is prepared by random positioning of water beads and Pluronic L64 chains. The number density (i.e. number of beads per unit volume) was set equal to 3 DPD units[1], meaning that the total number of beads was 81000.

The cut-off radius for non-bonded interactions was set equal to 1 with a timestep of 0.01 DPD units. Equilibrium only simulations were carried out for 2×10^6 timesteps, while non-equilibrium simulations were carried out for 3×10^5 followed by 5×10^5 timesteps applying different shear rates in different simulations. The range of concentrations spans from 5% to 95% in weight percentage (w/w) of Pluronic L64 and the range of non-dimensional DPD shear rates varies from 0.005 to 2. The DPD energy was set equal to 1 and its value was recorded every 500 timesteps. Moreover, the DPD property of preserving hydrodynamic interactions ensures that momentum is conserved across the box. The velocity Verlet algorithm was used as integration scheme. During the overall simulation time, energy was stable at $1.0 \pm 0.01\ k_B T$. A cluster analysis algorithm was written in Python[52] (Python Software Foundation, https://www.python,org/) in order to quantify modifications in the microstructure when shear is applied. The python code takes coordinates in input every 500 timesteps and a density-based algorithm captures the number of clusters/structures of the central hydrophobic part of the Pluronic L64 chain, while the other beads (i.e. water and PEO) are ignored. In such a way, it is possible to find specific patterns in the microstructures, such as formation of spherical micelles, soft-gel, hexagonal phase and lamellar structures. In equilibrium and non-equilibrium simulations, clusters are recognized according to a cutoff distance between closer beads. Closer neighbors are assigned to one single cluster and beads that are outside of the cutoff range are considered as belonging to other clusters. The expected total number of clusters is not known *a-priori*. The number of clusters was therefore monitored against the simulation time (for over 2×10^5 timesteps) in both the equilibrium and non-equilibrium stages. Also, the cluster size, quantified by the aggregation number, N, namely the number of Pluronic L64 chains in one cluster, was monitored and snapshots of the configuration of the system were stored. This data was then used to identify the cluster mass distribution (CMD) indicating how the population of clusters in the simulation box is distributed over the aggregation number N.

In the lower range of concentrations, the data collected during the cluster analysis was employed to calculate the micelles gyration radius and was used to determine their sphericity. It must be highlighted that, for complex structures, there is a correlation between the aggregation number and the gyration radius:

$$N = CR_g^d, \tag{12}$$

where N is the already introduced aggregation number, C is a constant, R_g is the gyration radius of the micelle and d is a scaling exponent, that tends to three in the case of spherical structures and tends to two in the case of cylindrical or worm-like structures. Plotting the aggregation number versus the radius of gyration (or viceversa) in a log-log scale allows to identify the value of the exponent d.

In non-equilibrium simulations, each system was initialized with a linear velocity profile, with the maximum desired velocity at the top of the box and zero velocity at the bottom (see for example Fig. S2 of the Supporting Information). Shear was only applied on the xz plane, meaning that only P_{xy}, one of the three non-diagonal component of the stress tensor, was not null. The velocity on the top slab was set equal to $\dot{\gamma}l$, where $\dot{\gamma}$ the DPD shear rate value and l is the length of the box. In this regime (i.e. from 0.005 to 2 DPD shear rate), a linear velocity profile was obtained for both a system containing only water and a mixture of water and Pluronic L64.

In order to ensure the validity of the results in the operative range, two sets of tests were performed for the upper and lower limits of the shear range. To set the upper limit, we observed the behavior of water viscosity, which needs to be consistent with its Newtonian nature (see Fig. S1 of the Supporting Information). However, for shear rate values greater than 2 DPD units an unphysical dependence of the viscosity on the shear rate is obtained. A shear rate of 1 DPD unit is therefore the maximum applicable in our simulation set up. It must be highlighted that, the set of parameters used to describe the Pluronic L64 chains is valid in equilibrium conditions and non-equilibrium parametrization may differ such that the predictions of some equilibrium properties could results in unrealistic values. The

shear rate in DPD units can be different from the physical shear rate at which an analogous situation is reached. When the value of the shear is greater than 1 DPD unit, the system could be exposed to extreme deformation that lead to non-physical results. To set the lower operating limit, velocity profiles across the simulation box at different shear rates were analyzed. When the shear value imposed on the system is around 10^{-3} DPD units, the thermal fluctuations due to the DPD thermostat are masking shear effects and the velocity profile is affected by beads, moving according to the temperature of the system. This effect was tested on both water and water-Pluronic L64 mixtures, therefore shear rate values smaller than 10^{-3} DPD units cannot be explored. Concluding, by using a conservative approach we can set the operating range of shear rates between 0.005 and 1 (see Figures reported in SI).

Viscosity was obtained averaging the value of the stress tensor P_{xy} every 100 timesteps. All the viscosity values are registered after an initial equilibration phase, such that initial fluctuations are filtered. The final value was recorded when fluctuations were around ± 0.01 μ_{DPD}, by adjusting the simulation time window. In particular, the trend of the viscosity was recorded during the simulation time and the final value recorded only when fluctuations were in the order of magnitude of 0.01 μ_{DPD}. The harmonic potential was finely tuned in order to suppress the formation of over-elongated chains, hence the K_{Harm} coefficient was initially set equal to 4.0 (in DPD units) and then modified[4]. One concentration (i.e. 25% w/w of Pluronic L64 in water) was used as a sample and K_{Harm} was increased until variations in the viscosity were negligible. In order to reduce potential errors due to extreme shear conditions and over-elongation, the same set of parameters used for the harmonic potential was used in the FENE potential simulations, this means that the value of the spring constant, K_{FENE} , was set equal to 50 DPD units, while the equilibrium distance, r_e, was set equal to 1.00 DPD units. Rheograms were obtained for different concentrations of Pluronic L64 at different shear rates, recording the value of viscosity every 0.01 DPD shear units. The qualitative variation of the trend of the viscosity was proven to be related to differences in the microstructure.

Simulations were performed on a cluster InfiniBand 4 TFLOPS on 10 cores AMD Bulldozer and 128GB of RAM.

4. Results and discussion

In this section, we present the results obtained running DPD simulations for mixtures of water and Pluronic L64 at different concentrations. The first part focuses on the comparison between predictions obtained with equilibrium DPD simulations, on the whole spectrum of Pluronic L64 concentrations, with the experimentally observed structures[49], whereas the second part shows the effect of shear, investigated with non-equilibrium DPD simulations.

Equilibrium simulations.

Equilibrium DPD simulations have been performed keeping the temperature bounded at around k_BT = 1.00 DPD units (corresponding to *298* K and indicated as a red line in Figure 1). Snapshots of the DPD simulations are reported in Figure 1, which includes also the experimentally measured phase diagram. As it can be qualitatively appreciated, peculiar microstructures emerge while concentration increases. Above the critical micellar concentration (CMC), nearly spherical micelles are present at low concentration (below 25% w/w), while elongated structures can be appreciated at slightly higher concentrations. The presence of a structured network is found when the Pluronic L64 concentration is above 40% w/w, resembling the structure of a soft-gel, while clear lamellar structures are obtained between 70% and 80% w/w. At very high concentrations (i.e. above 85% w/w) small clusters of water are trapped into a Pluronic L64 network, corresponding to the so-called reverse micelles. Closer observation of Figure 1 confirms that these findings are in good agreement with the measured phase diagram. The length of the box ensures that enough structures (i.e. number of micelles, hexagons and layers in lamellar phase) are obtained to avoid simulation artifacts. As previously discussed, different lengths of the box were tested and an optimal compromise between simulation time and reduction of artifacts was found in the $30\times r_c$ box.

In order to quantitatively characterize the different microstructures, the data collected from the cluster analysis was also used. Figure 2 reports for example, in the concentration range between 5% and 25% w/w of Pluronic L64, the values of the calculated radius of gyration of micelles detected at different time instants of the DPD simulation plotted versus their aggregation numbers, together with a red line, indicating a slope of 1/3 (corresponding to a scaling exponent *d* of three in Eq. 12) and a yellow line, indicating a slope of ½ (corresponding to a value of the scaling exponent *d* of two in Eq. 12).

As it is possible to see by increasing the Pluronic L64 concentration larger micelles are formed, as confirmed also by Fig. 3, which shows also that the number of micelles formed increases with the Pluronic L64 concentration. Figure 2 shows also that, at the lowest concentrations and for aggregation numbers greater than four, the micelles radius of gyration scales with the aggregation number with an exponent of $d=3$, highlighting the presence of nearly spherical micelles. However, for the largest concentration of polymer that still allows micellar structures to form (e.g. 25% w/w), the clusters characterized by higher aggregation numbers (above 100) change their geometry from spherical (d=3) to cylindrical (d=2), clearly indicating the emerging of elongated micelles.

The data collected from the cluster analysis also confirmed that when the concentration of Pluronic L64 is greater than 40% micelles undergo a transition from spherical to elongated structures[53], resulting eventually in the formation of a bi-continuous phase. An example is shown in Fig. 4 (left) for a Pluronic L64 concentration of 60% w/w. Finally, at even higher concentrations, lamellae can be observed, but they are not properly identified by the clustering algorithm due to small interconnections between them. More quantitative results from the cluster analysis will be discussed in the next section, together with the non-equilibrium simulations.

Non-equilibrium simulations.

As already mentioned non-equilibrium DPD simulations were used to explore qualitative drawbacks of shear on the observed microstructures focusing on the variation of the apparent viscosity, number

and dimension of microstructure as a function of the applied shear. Different batches of simulations were run using Harmonic and FENE potentials.

In a DPD model, the parameters for the non-bonded forces are normally selected based on thermodynamic properties such as solubility coefficients or compressibility data[1]. However, a specific criterion to select the bonded parameter (especially when shear is applied) has not been established yet. We decided to tune the value of the harmonic constant, monitoring the viscosity values. A fairly weak spring constant was initially selected, keeping the equilibrium distance equal to 1.00 according to the literature[50], and then gradually increased. The resulting viscosity values at different shear rates were then recorded and plotted (Figure 5). When the spring value crossed 50 DPD units limit, the viscosity was not affected anymore by increasing it further. Once this limit was found, before starting non-equilibrium simulations, the FENE potential was used to describe the bonded potential using the same set of parameters obtained from the fine tuning of harmonic potential. This was done in order to reduce over-elongation of the chains when shear values were high. A comparison between results obtained with the two potentials at different Pluronic L64 concentrations and different shear rates is summarized in Figure 6. As it is clear, small deviation in numerical values are present, but the emerging rheological behavior is similar for both cases. The value of the constants used to describe the FENE potential are K_{FENE} equals to 50 DPD units and r_e equals to 1.00 DPD units. Now that the bonded parameters have been chosen, we can investigate the effect that shear rate and polymer concentration have on the viscosity and the microstructure of the liquid.

Figure 7 shows how the viscosity changes with the shear rate at different Pluronic L64 concentrations, ranging from 0% (pure water) to 85% w/w. As expected for pure water no changes in the apparent viscosity are observed, whereas with increasing the Pluronic L64 concentration, the mixture develops a shear-thinning behavior, which becomes more pronounced as the polymer concentration increases. The soft-gel structure, obtained at a concentration equals to 60%, when shear rate is applied on the system, is destroyed and an ordered hexagonal phase, constituted by long elongated cylinders

perfectly aligned to the streaming flow, emerges. Because of this structural change, a qualitative drop in the viscosity of the fluid can be observed.

Deviation from the equilibrium configurations.

In this section we quantify shear effects on microstructures by using the cluster analysis. One example was already reported in Fig. 4, where the formation of the hexagonal phase was qualitatively observed at a Pluronic L64 concentration of 60% by weight under a shear rate of 0.1 DPD units. In Figure 8, the number of polymer clusters, calculated with the clustering algorithm, is plotted against the simulation time, for three different Pluronic L64 concentrations, representative of three different microstructures, with and without shear acting on the simulation box. The shear rate used in this example is an intermediate value of 0.1 DPD units, far from both the extremely high and extremely low shear regions. Results obtained at other shear rate values led to very similar results. The figure reports simulations obtained with an equilibration phase of 3×10^5 DPD timesteps, but tests performed with longer equilibration phases (i.e., 2×10^6 timesteps) and the application of shear for longer times (up to 2×10^6 timesteps) did not provide relevant differences. As already mentioned, the reported results refer to a size of $30\times r_c$ always leading to the formation of numerous clusters. As it can be seen from Figure 8, when the Pluronic L64 concentration is around 25% w/w, after an initial transitory phase, in which the randomly positioned chains get closer to each other, spherical micelles are formed, and equilibrium is reached. When shear (represented by the region between the red dashed lines) is applied on the box, its streaming effect induces coalescence between micelles that are close to each other, as proven by the slight reduction in the number of detected micelles/clusters[54].

When the Pluronic L64 concentration is equal to 45% w/w and no shear is applied a soft-gel is formed and the clustering algorithm detects only one or two clusters. When shear is applied cylindrical micelles appear, arranged in a hexagonal structure, causing a significant increase in the total number of detected cluster, as clearly visible in Figure 8 (and in Fig. 4). Similar conclusions can be drawn

also for the highest Pluronic L64 concentration (i.e., 75% w/w) for which an increase in the observed number of clusters is visible when the shear is applied.

These modifications in the structures due to shear are also highlighted in Figure 9 where for three different Pluronic L64 concentrations the observed cluster are reported at equilibrium (top) and under shear (bottom). As seen for the lowest concentration the application of shear simply induces micelle coalescence. When the concentration is increased up to 45% w/w at equilibrium one unique cluster is detected and when shear is applied the network breaks and hexagonal oriented structures are formed. Finally, the same idea applies to the lamellar phase encountered when the Pluronic L64 concentration is increased up to 75% w/w. At this concentration the clustering algorithm detects one (or few) cluster, as it is difficult to count the number of lamellas at equilibrium due to interconnections. As visible from Figure 9 shear is able to break the structure increasing the number of lamellas.

These observations are quantified in Figure 10 that shows the cluster mass distributions (CMD), expressed as the frequency of detected structures versus the aggregation number, for the three Pluronic L64 concentrations of 25% w/w, 45% w/w and 75% w/w with and without shear. As it can be seen, application of shear at the lowest concentration slightly changes the CMD, resulting in the formation of larger (spherical) micelles and increasing the cluster size (or aggregation number) from 30-40 to 60-80. Both at 45% and 75% w/w the presence of one large cluster or a few larger clusters is detected without shear and the application of shear induces the formation of a few smaller structures.

5. Conclusions

In this study, we simulated the entire phase diagram of a structured fluid, composed of Pluronic L64 and water by using DPD. We were able to recognize the peculiar structures that form when the concentration varies from dilute to dense, namely spherical and rod-like micelles, hexagonal and lamellar phases, as well as reverse micelles. Results on this part of the work were found in good agreement with experiments. A novel clustering algorithm was used to identify the structures formed, characterize them in terms of radius of gyration and aggregation number and cluster mass distributions.

Eventually non-equilibrium simulations were also performed, in order to predict how structures are affected by shear, both via qualitative and quantitative analyses. We had to tune bonded interactions between beads, belonging to the same chain, because we noticed that weak springs were affecting the overall behavior of macroscopic dynamic properties when shear was applied. Two different types of potential were tested and tuned in order to limit this effect. We acknowledge that further investigation is needed to understand differences in the numerical values.

Despite the well-known scaling problem that result in unrealistic shear rates in real units (similarly to what happens in non-equilibrium AAMD), we proved that non-Newtonian behaviors can be predicted by DPD and associated to variations of the observed microstructures. Evident drops have been highlighted at higher concentrations, where a transition between phases was more evident.

We are now investigating different species of Pluronic, using the same set of parameters we already used, as ensuring that the parameters are applicable to different Pluronic will assess the portability of the DPD model to other chemical systems.

6. Acknowledgements

Computational resources were provided by HPC@POLITO, a project of Academic Computing within the Department of Control and Computer Engineering at the Politecnico di Torino (http://www.hpc.polito.it). The authors want to thank Prof. Mike Allen for the useful discussion on scaling factors and clustering algorithm. One of the authors (IP) acknowledges MINECO and DURSI for financial support under projects FIS2015-67837-P and 2014SGR-922, respectively.

References

[1] R.D. Groot, and P.B. Warren, J. Chem. Phys., **107**, 4423 (1997).

[2] A. Prhashanna, S. A. Khan, and S. B. Chen, Colloids Surf. A Physicochem. Eng. Asp., **506**, 457 (2016).

[3] F. Cheng, X. Guan, H. Cao, T. Su, J. Cao, and Y. Chen, Int. J. Pharm., **492**, 152 (2015).

[4] X. Cao, G. Xu, Y. Li, and Z. Zhang, J. Phys. Chem. A, **109**, 10418 (2005).

[5] L. Zhen, K. Liu, D. Huang, X. Ren, R. and Li, J. Dispersion Sci. Technol., **37**, 941 (2016).

[6] Y. Li, H. Zhang, M. Bao, and Q. Chen, J. Dispersion Sci. Technol., **33**, 1437 (2012).

[7] B. Wang, Y. Shang, H. Liu, and Y. Hu, Fluid Phase Equilib., **228-229**, 109 (2012).

[8] G. E. Son, N. Sugartseren, W. Yoon, and S. K. Kwak, J. Chem. Eng. Data, **59**, 3036 (2014).

[9] S. Yuan, Z. Cai, G. Xu, and Y. Jiang, Chem. Phys. Lett., **365**, 347 (2014).

[10] L. Gentile, M. A. Behrens, S. Balog, K. Mortensen, G. A. Ranieri, and U. Olsson, J. Phys. Chem. B, **118**, 3622 (2014).

[11] S. C. Mehta, P. Somasundaran, and R. Kulkarni, J. Colloid Interface Sci., **333**, 635 (2009).

[12] V. M. Sadtler, M. Guely, P. Marchal, and L. Choplin, J. Colloid Interface Sci., **270**, 270 (2004).

[13] G. E. Newby, I. W. Hamley, S. M. King, C. M. Martin, and N. J. Terrill, J. Colloid Interface Sci., **329**, 54 (2009).

[14] M. Youssry, F. Asaro, L. Coppola, L. Gentile, and I. Nicotera, J. Colloid Interface Sci., **342**, 348 (2010).

[15] Y. Suganuma, M. Imai, T. Kato, U. Olsson, and T. Takahashi, Langmuir, **26**, 7988 (2010).

[16] S. C. Sharma, L. K. Shrestha, K. Tsuchiya, K. Sakai, H. Sakai, and M. Abe, J. Phys. Chem. B, **113**, 3043 (2009).

[17] L. Gentile, B. F. B. Silva, S. Balog, K. Mortensen, and U. Olsson, J. Colloid Interface Sci., **372**, 32 (2012).

[18] Y. Meng, D. Gu, F. Zhang, Y. Shi, L. Cheng, D. Feng et al., Chem. Mater., **18**, 4447 (2006).

[19] P. Alexandridis, U. Olsson, and B. Lindman, Langmuir, **14**, 2627 (1998).

[20] P. Holmqvist, P. Alexandridis, and B. Lindman, J. Phys. Chem. B, **102**, 1149 (1998).

[21] P. Alexandridis, U. Olsson, and B. Lindman, Macromolecules, **28**, 7700 (1995).

[22] R. Ivanova, B. Lindman, and P. Alexandridis, Langmuir, **16**, 9058 (2000).

[23] R. Ivanova, P. Alexandridis, and B. Lindman, Colloids Surf. A Physicochem. Eng. Asp., **183**, 41 (2001).

[24] B. Svensson, P. Alexandridis, and U. Olsson, J. Phys. Chem. B, **102**, 7541 (1998).

[25] D. Zhou, P. Alexandridis, and A. Khan, J. Colloid Interface Sci., **183**, 339 (1996).

[26] J.S. Nambam, and J. Philip, J. Phys. Chem. B, **116**, 1499 (2012).

[27] B. Sarkar, V. Ravi, and P. Alexandridis, J. Colloid Interface Sci., **390**, 137 (2013).

[28] K. Aramaki, M. K. Hossain, C. Rodriguez, M. H. Uddin, and H. Kunieda, Macromolecules, **36**, 9443 (2003).

[29] V. Castelletto, P. Parras, I. W. Hamley, P. Bäverbäck, J. S. Pedersen, and P. Panine, Langmuir, **23**, 6896 (2007).

[30] X. Li, Y. Huang, X. Chen, Y. Zhou, Y. Zhang, P. Li et al., J. Drug Targeting, **17**, 739 (2009).

[31] N. Ghaouar, M. B. Henda, A. Aschi, and A. Gharbi, J. Macromol. Sci. Part B Phys., **50**, 2150 (2011).

[32] Y. W. Jung, H. Lee, J. Y. Kim, E. J. Koo, K. S. Oh, and S. H. Yuk, Curr. Med. Chem., **20**, 3488 (2013).

[33] L. Fan, M. Degen, N. Grupido, S. Bendle, and P. Pennartz, Mater Sci. Eng. A, **528**, 127 (2010).

[34] M. Impéror-Clerc, S. Manet, I. Grillo, D. Durand, A. Khodakov, and V. Zholobenko, Stud. Surf. Sci. Catal., **174**, 805 (2010).

[35] F. Aydin, X. Chu, G. Uppaladadium, D. Devore, R. Goyal, N. S. Murthy et al., J. Phys. Chem. B, **120**, 3666 (2016).

[36] N. Sun, Y. Li, D. Wang, M. Bao, and L. Tong, Acta Chim. Sin., **71**, 186 (2013).

[37] M. Elluru, H. Ma, M. Hadjiargyrou, B.S. Hsiao, and B. Chu, Polymer, **54**, 2088 (2013).

[38] M. Almgren, W. Brown, and S. Hvidt, Colloid Polym. Sci., **273**, 2 (1995).

[39] X. Cao, G. Xu, Y. Li, and Z. Zhang, J. Phys. Chem. A, **109**, 10418 (2005).

[40] X. Song, S. Zhao, S. Fang, Y. Ma, and M. Duan, Langmuir, **32**, 11375 (2016).

[41] D. Nicolaides, Mol. Simul., **26**, 51 (2001).

[42] X. Zhou, X. Wu, H. Wang, C. Liu, and Z. Zhu, Phys. Rev. E Stat. Nonlinear Soft Matter Phys., **83,** 041801 (2011).

[43] P. J. Hoogerbrugge, and J. M. V. A Koelman, EPL, **19**, 155 (1992).

[44] P. Español, and P. B. Warren, Journal of Chemical Physics, **146,** 150901 (2017).

[45] I. Pagonabarraga, and D. Frenkel, J. Chem. Phys., **115**, 5015 (2001).

[46] I. Pagonabarraga, and D. Frenkel, Mol. Simul., **25**, 167 (2000).

[47] S. Chen, N. Phan-Thien, X. Fan, and B. C. Khoo, J. Non-Newton Fluid Mech., **118**, 65 (2000).

[48] S. Meng, J. Zhang, Y. Wang, X. Li, C. Wu, T. Hou et al., Mol. Simul., **41**, 772 (2015).

[49] A. W. Lees, and S. F. Edwards, Journal of Physics C: Solid State Physics, **5**, 1921 (1972).

[50] S. Plimpton, J. Comput. Phys., **117**, 1 (1995).

[51] W. Humphrey, A. Dalke, and K. Schulten, J. Mol. Graph., **14**, 33 (1996).

[52] F. Pedregosa, G. Varoquaux, A. Gramfort, V. Michel, B. Thirion, O. Grisel et al., J. Mach. Learn. Res., **12**, 2825 (2011).

[53] M.S. Turner, and M.E. Cates, J. Phys: Condens. Matter, **4**, 3719 (1991)

[54] S.Q. Wang, M.W Gelbart, and A. Ben-Shaul, J, Phys. Chem., **6**, 2219 (1990)

TABLE I.

Conservative soft potential parameters a_{ij} expressed in DPD units for water/Pluronic L64 system. For similar species, values are obtained by scaling the isothermal compressibility of the water, while for different species an extra contribute, due to the solubility, is added.

	Water (*i*=1)	**A (*i*=2)**	**B (*i*=3)**
Water (*j*=1)	25	25.9	48.9
A (*j*=2)	25.9	25	38.4
B (*j*=3)	48.9	38.4	25

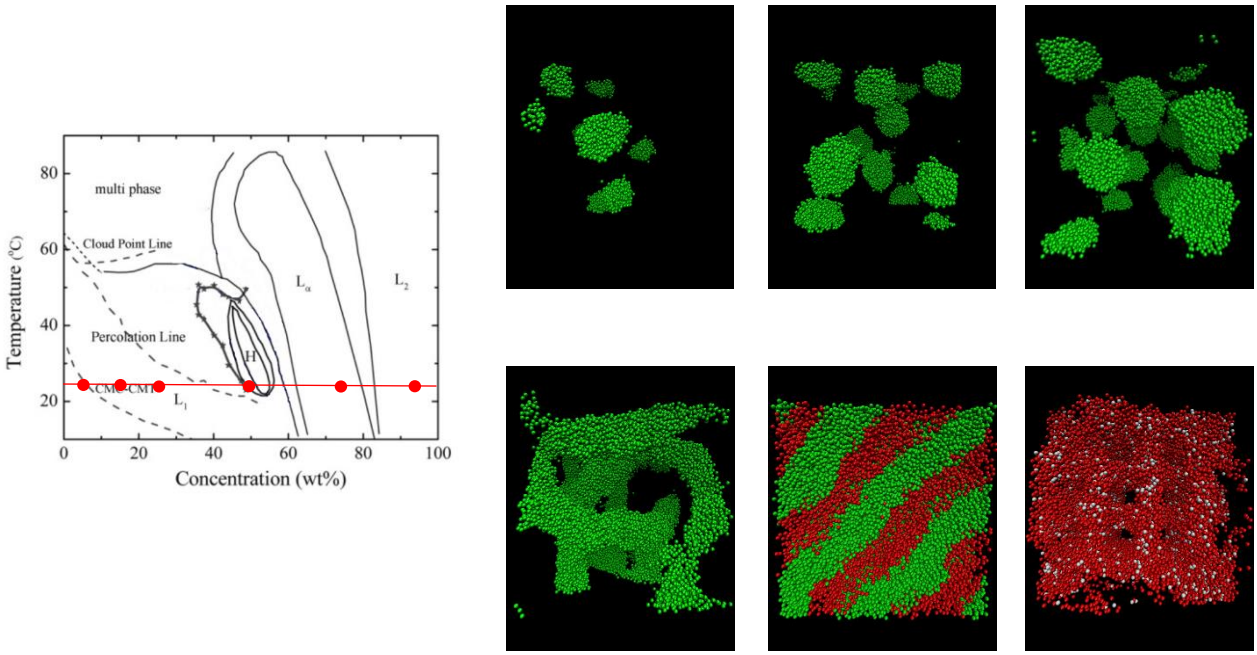

FIG. 1. Left: experimentally measured phase diagram for Pluronic L64 and water[42]. L_1 is for the micellar phase, H for the hexagonal phase, L_α for the lamellar phase and L_2 for the reverse micellar phase. The red line indicates the investigated temperature. Right: selected snapshots of DPD equilibrium at different Pluronic L64 concentrations (from left to right and top to bottom: 5%, 15%, 25%, 50%, 75% and 95%). Green beads represent PPO, red beads PEO and white beads water and until 40%, only PPO beads are shown. In the last snapshot, only PEO and water beads are shown.

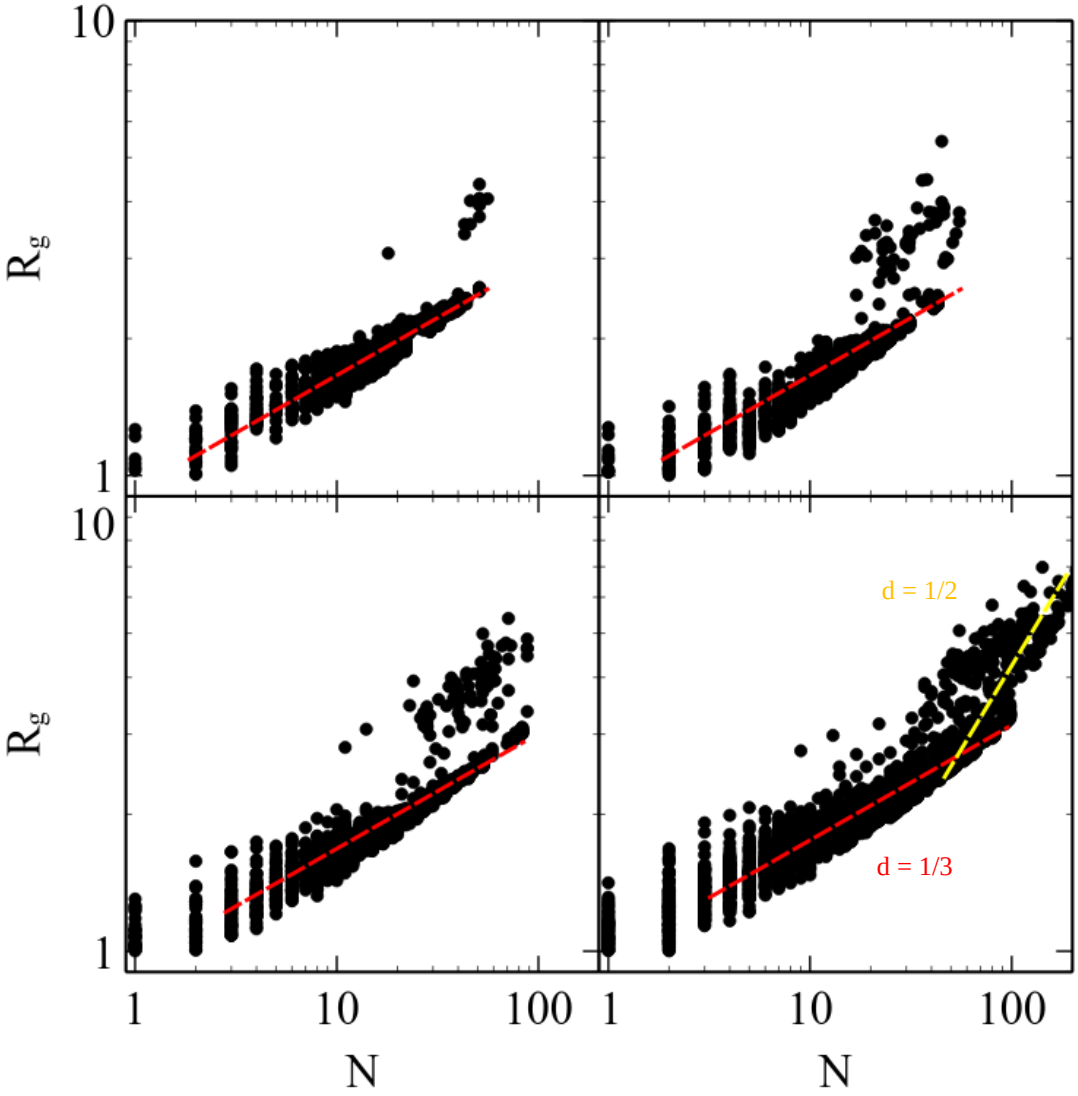

FIG. 2. From left to right and top to down gyration radii are plotted against the aggregation number for 5%, 10%, 15%, and 25% w/w of Pluronic L64. The red dashed line indicates a slope of 1/3 whereas the yellow dashed line indicates a slope of ½.

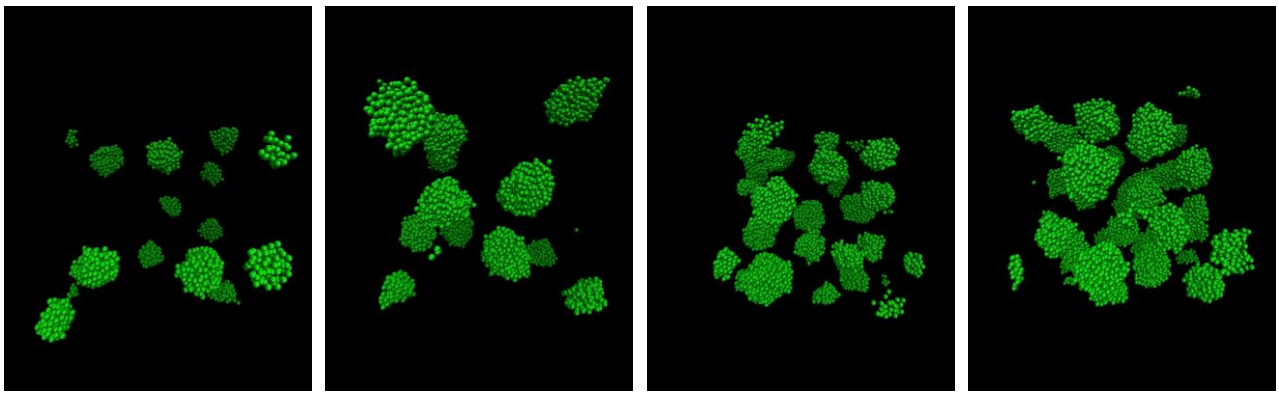

FIG. 3. Observed microstructures at, from left to right, 5%, 10%, 15% and 25% w/w. Green beads represent of the PPO part of the Pluronic L64, while water and PEO beads are not shown.

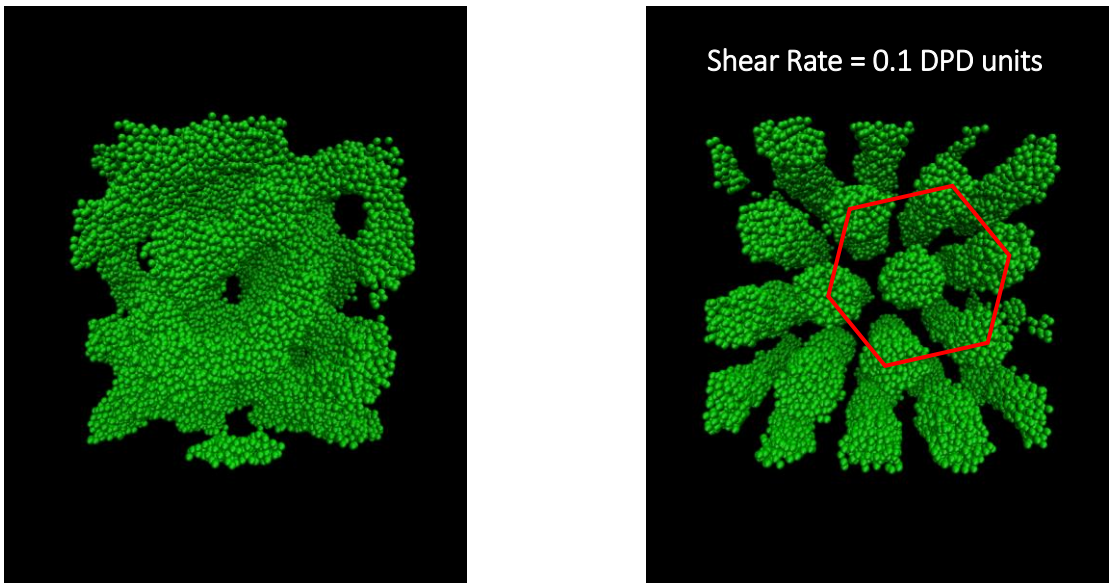

FIG. 4. Snapshots of the DPD simulations for a Pluronic L64 concentration of 60% w/w. An interconnected structure can be observed at equilibrium (left), while the hexagonal phase can be appreciated when the system undergoes shear (right) with a shear rate of 0.1 DPD units.

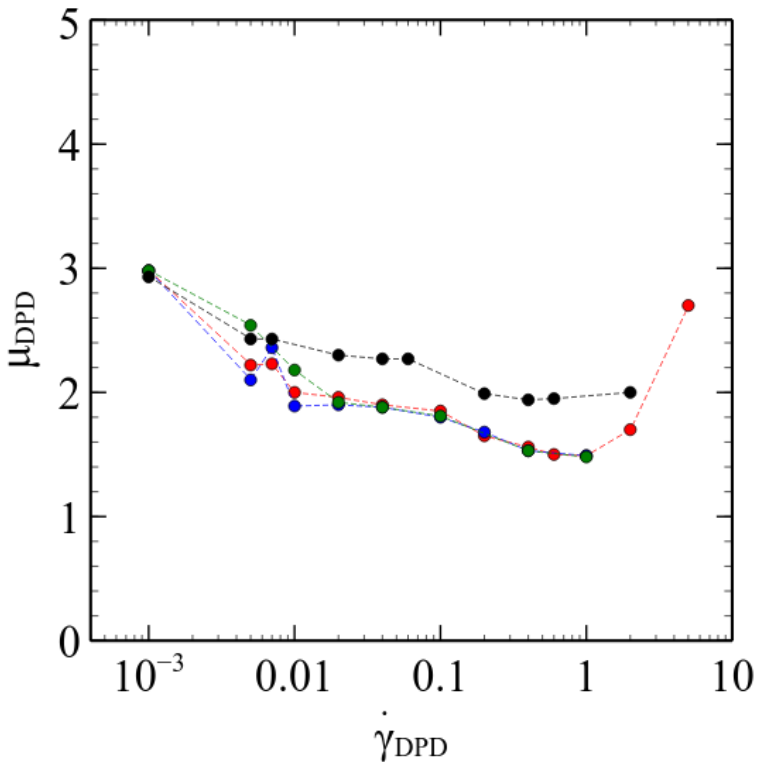

FIG. 5. Viscosity (in DPD units) versus shear rate (in DPD units) using harmonic potential at different K_{Harm} constants (black: 4.0, green: 50.0, blue: 100.0, red: 200.0). The tested system is composed by water and 25% of Pluronic L64 in a box with length equals to 30×r_c.

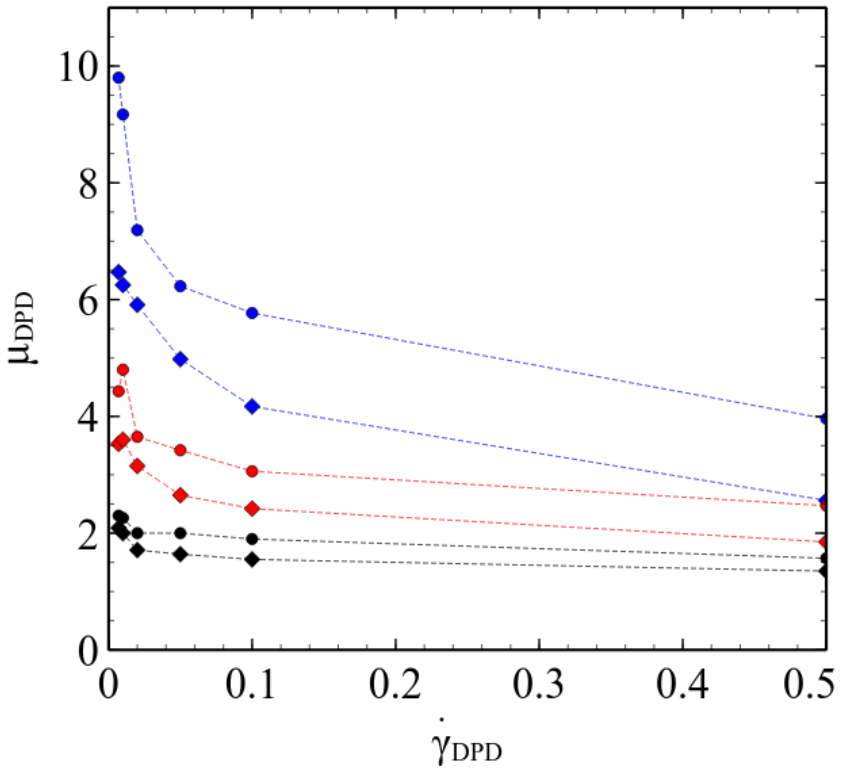

FIG. 6. – Comparison between viscosities obtained using Harmonic (filled circles) and FENE (filled diamonds) potentials at different concentrations w/w (black: 25%, red: 45%, blue: 75%) of Pluronic L 64 in water as a function of the shear rate. K_{Harm} *and* K_{FENE} *are equal to 50 DPD units,* r_e *is equal to 1.00 DPD units for both cases. Quantities are reported in DPD units.*

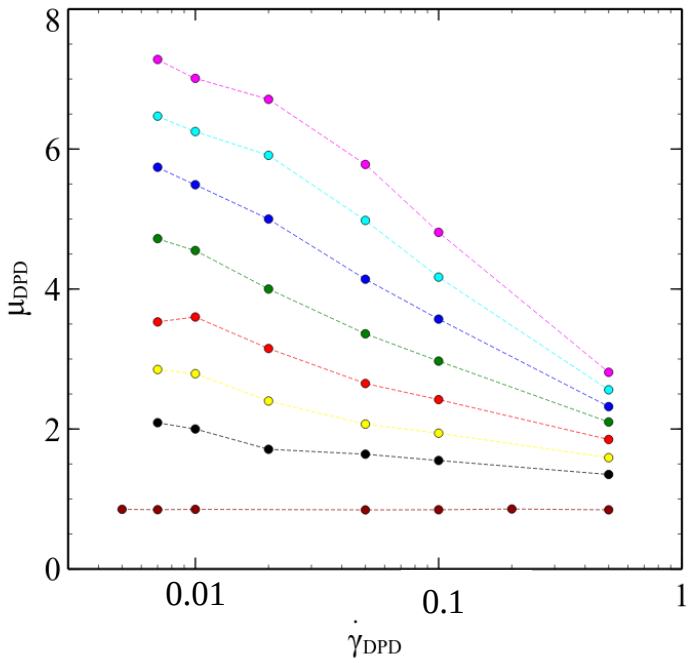

FIG. 7. Variation of the viscosity (in DPD units) as a function of the shear rate (in DPD units) at different Pluronic L64 concentrations w/w (amaranth: 0%, black: 25%, yellow: 35%, red: 45%, green: 55%, dark blue: 65%, light blue: 75%, purple: 85%).

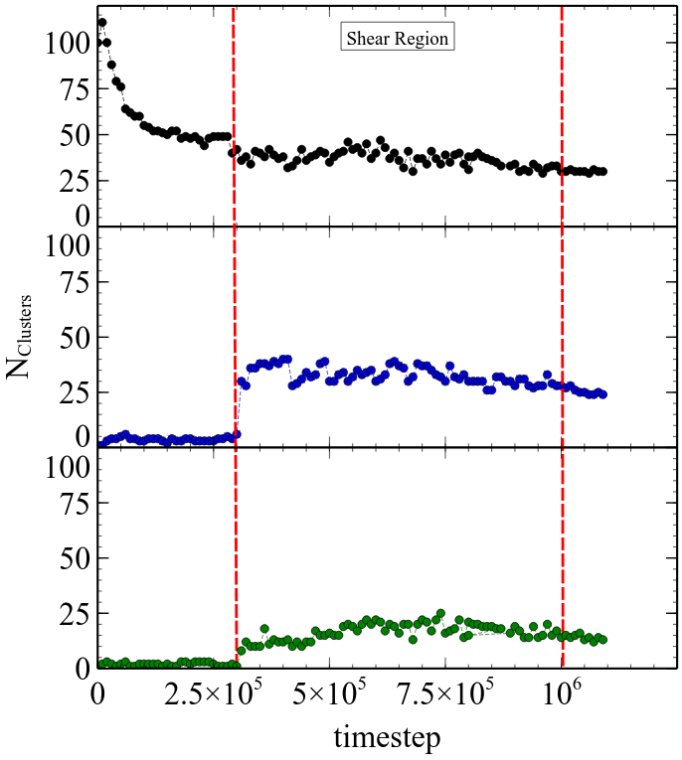

FIG. 8. Time evolution of the number of detected clusters in the simulation box for three different Pluronic L64 concentrations of 25% w/w (black), 45% w/w (blue) and 75% w/w (green). Red dashed lines represent the interval in which shear was applied on the simulation box

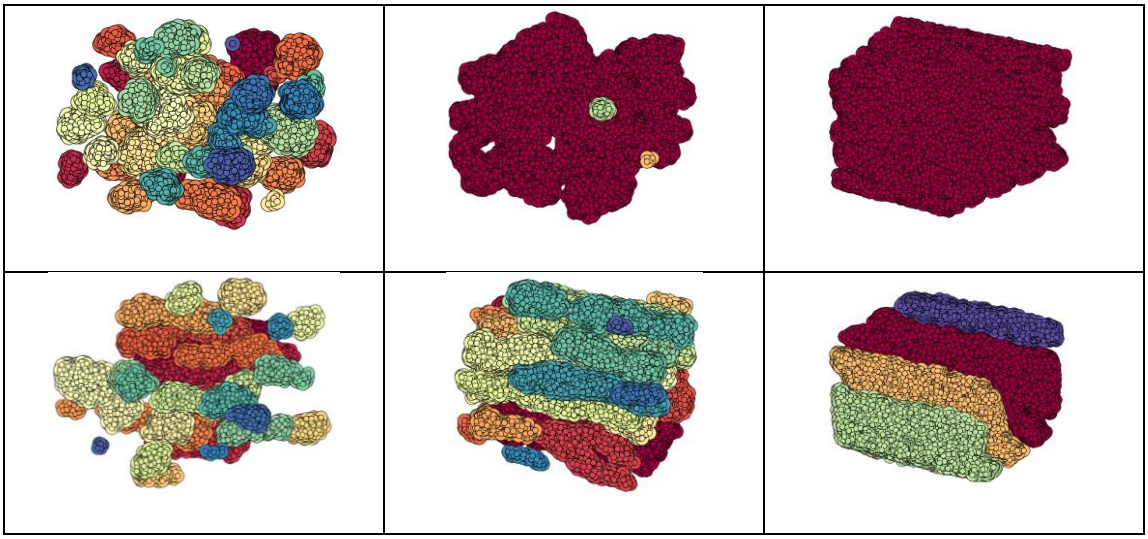

FIG. 9. DPD simulation snapshots for different Pluronic L64 concentrations (from left to right: 25% w/w, 45% w/w and 75% w/w) at equilibrium (top) and non-equilibrium (bottom). The shear rate is equal to 0.1 DPD units and only PPO part of the co-polymer is shown. Different colors represent different clusters found by the clustering algorithm.

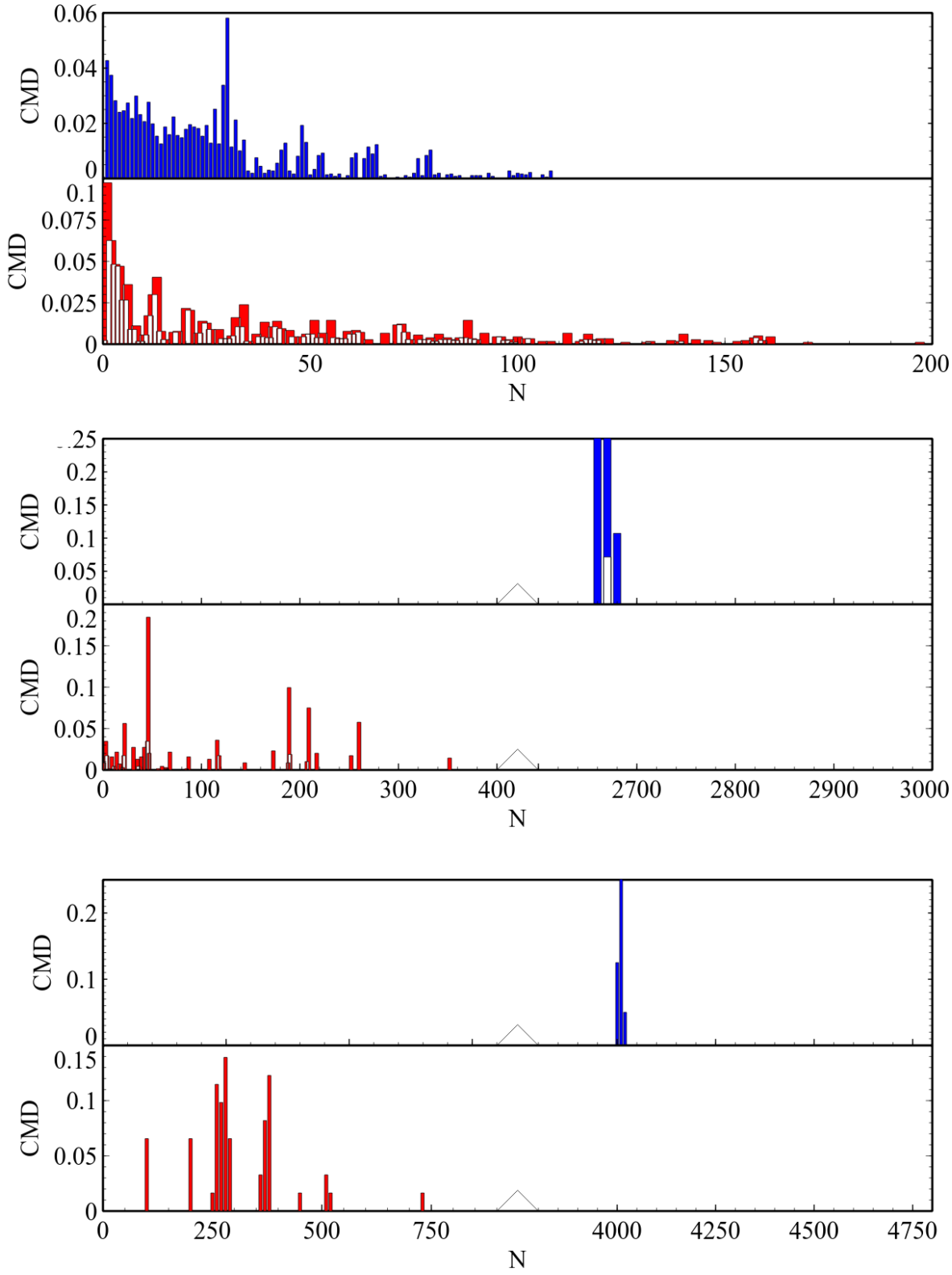

FIG. 10. - Cluster mass distribution (CMD) plotted versus the cluster size or aggregation number detected at equilibrium (top plots in blue) and when shear of 0.1 DPD units is applied (bottom plots in red) for (from top to bottom) Pluronic L64 concentration of 25% w/w, 45% w/w and 75% w/w.

Supporting Information

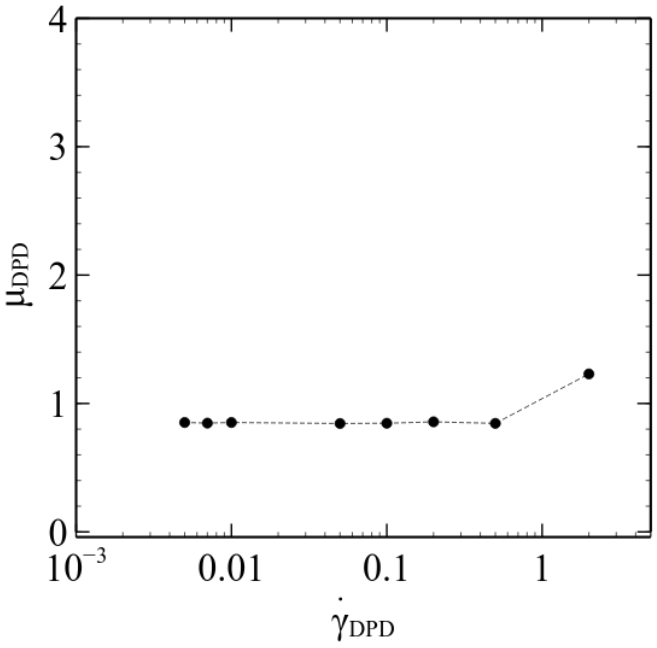

FIG. S1. Viscosity coefficient (in DPD units) plotted against shear rate (in DPD units) as measured from non-equilibrium DPD simulations. Viscosity was recorded every 1000 DPD timesteps after an initial equilibration phase and only the average value is reported.

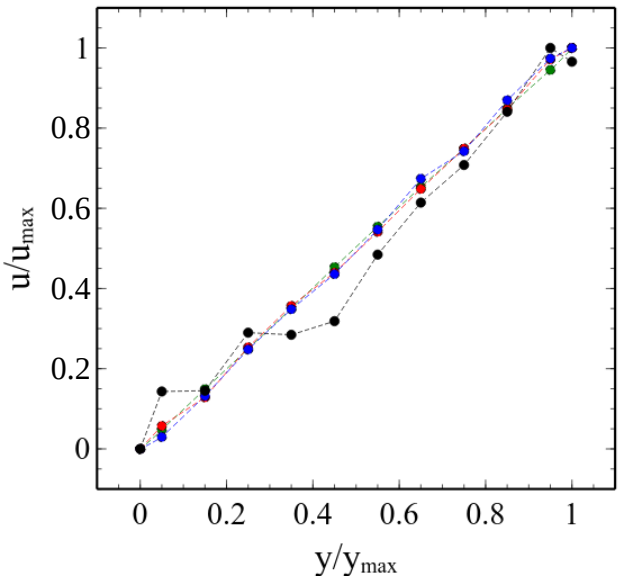

FIG S2. Velocity profiles developed along the y-coordinate of the simulation box for a system containing only water beads. The values of the velocity and the y-coordinate are normalized to their maximum value. Different shear rates (black: 0.005, blue: 0.02, red: 0. 2, green: 2.0) correspond to different velocities.